

# D-Wave Phonon Angular Momentum Texture in Altermagnets by Magnon-Phonon-Hybridization

Hannah Bendin<sup>1,2</sup>, Alexander Mook<sup>3,4</sup>, Ingrid Mertig<sup>1</sup> and Robin R. Neumann<sup>3,4,1,\*</sup>

<sup>1</sup>*Institute of Physics and Halle-Berlin-Regensburg Cluster of Excellence CCE, Martin Luther University Halle-Wittenberg, D-06099 Halle (Saale), Germany*

<sup>2</sup>*Institute of Physics, Otto von Guericke University Magdeburg, D-39106 Magdeburg, Germany*

<sup>3</sup>*Institute of Solid State Theory, University of Münster, D-48149 Münster, Germany*

<sup>4</sup>*Institute of Physics, Johannes Gutenberg University Mainz, D-55128 Mainz, Germany*

(Dated: November 12, 2025)

In altermagnets, the magnon bands are anisotropically spin-split in reciprocal space without relativistic or dipolar spin-spin interactions. In this work, we theoretically study magnons and phonons coupled by spin-lattice interaction in a two-dimensional square-lattice  $d$ -wave altermagnet. We show that phonon-chirality-selective magnon-phonon hybridization can be caused by interfacial Dzyaloshinskii-Moriya interaction leading to the emergence of hybrid quasiparticles that possess finite phonon angular momentum. These hybrid quasiparticles are called magnon polarons and consist of spin-polarized magnons and chiral phonons. Their phonon angular momentum texture follows the  $d$ -wave character of the magnon spin texture opening up the possibility of phononic counterparts to the electronic response effects in altermagnets, such as a *phonon angular momentum splitter effect*, i.e., the generation of a transverse phonon angular momentum current induced by a temperature gradient – the bosonic analogue of the spin-splitter effect.

**Introduction.** Chiral phonons [1–3], the quasiparticles of circularly polarized lattice vibrations, have recently been investigated due to a range of emerging phenomena. They have been found to contribute to spin relaxation [4, 5], ultrafast demagnetization [6, 7] and the Einstein-de Haas effect [8, 9]. Notably, chiral phonons carry nonzero angular momentum and can therefore function as angular momentum carriers in non-magnetic materials [10, 11]. Here we are using the term “chiral phonon” synonymously to “axial phonon” proposed in Ref. [12] for phonons that carry angular momentum.

The systems in which chiral phonons occur still require extensive research. Chiral phonons may, for example, be found in lattices with broken inversion symmetry [1, 2, 13–15]. Due to the preserved time-reversal symmetry, the phonon angular momentum has an odd parity:  $L(\mathbf{k}) = -L(-\mathbf{k})$  [14]. In order to realize *even-parity* textures, time-reversal symmetry must be broken [14], e.g., by the coupling to magnons, the quasiparticles of spin excitations [16–22].

In this work, we delineate an approach to design even-parity phonon angular momentum textures beyond  $s$ -wave. Our approach is based on a chirality-selective magnon-phonon coupling, which leads to the hybridization between magnons and phonons. In particular, we show that the strength of magnon-phonon coupling originating from interfacial Dzyaloshinskii-Moriya interaction (DMI) depends on the magnon spin and the phonon angular momentum. We study their hybridization in the context of a  $d$ -wave altermagnet [23, 24] and demonstrate how the symmetry of the magnon spin texture can be imprinted onto the phonon angular momentum texture of the emergent magnon polarons (cf. Fig. 1). Our findings encourage the exploration of the vibrational degrees of freedom in novel unconventional magnetic phases such as altermagnets or antialtermagnets [25] and highlight the potential of unconventional magnetism for realizing chiral phonons.

**Results.** We consider the minimal, two-dimensional altermagnet depicted in Fig. 2(a) with the two sublattices  $\uparrow$  (red

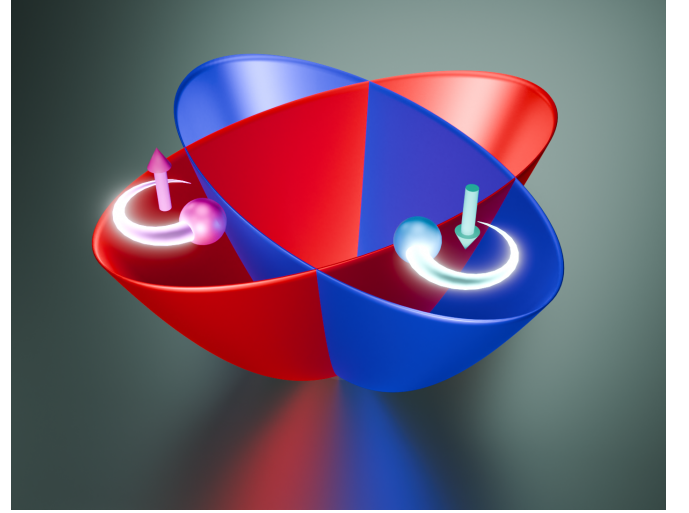


FIG. 1. Visualization of the generation of phonon angular momentum in altermagnets through the coupling with the underlying spin-split magnon band structure. Their hybridization selectively depends on the circular polarization of the phonons and, thus, it separates left- and right-handed phonons imprinting an alternating phonon angular momentum texture in reciprocal space.

circles) and  $\downarrow$  (blue circles). The localized spins assume a collinear Néel order and interact via antiferromagnetic nearest and anisotropic ferromagnetic next-nearest neighbor Heisenberg coupling. These ingredients are encompassed by the Hamiltonian

$$\hat{H}_m = -\frac{J_{\text{AFM}}}{2} \sum_{\langle i,j \rangle} \mathbf{S}_i \cdot \mathbf{S}_j - \frac{J_{\text{FM}_1}}{2} \sum_{\langle\langle i,j \rangle\rangle_1} \mathbf{S}_i \cdot \mathbf{S}_j - \frac{J_{\text{FM}_2}}{2} \sum_{\langle\langle i,j \rangle\rangle_2} \mathbf{S}_i \cdot \mathbf{S}_j. \quad (1)$$

Here,  $J_{\text{AFM}} < 0$  and  $J_{\text{FM}_{1,2}} > 0$  describe the antiferromagnetic and ferromagnetic interaction, respectively.  $\langle i, j \rangle$  runs over

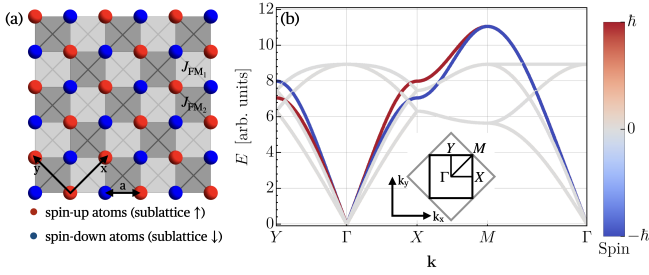


FIG. 2. (a) Illustration of the minimal altermagnetic model. It comprises antiferromagnetic nearest-neighbor interactions and directional, ferromagnetic next-nearest neighbor interactions as indicated by the gray checkerboard pattern. (b) Magnon and phonon modes in the absence of spin-lattice coupling. The color indicates the magnon spin. Thus, the phonon modes are depicted in gray while the red and blue colors confirm the spin-dependent splitting of the magnon modes. Along the nodal lines  $\overline{\Gamma M}$  the two magnon bands are degenerate. Inset: Brillouin zone of the magnetic (structural) unit cell shown in black (gray). (The coordinate systems of the real and reciprocal spaces are rotated by  $45^\circ$  to each other.) The parameters used for the calculations are  $J_{\text{AFM}} = -1$ ,  $J_{\text{FM}_1} = 0.383$ ,  $J_{\text{FM}_2} = 0.5$ , and  $S = 1$ .

all nearest neighbors, while  $\langle\langle i, j \rangle\rangle_i$  runs over all next-nearest neighbors with bonds located within light gray ( $i = 1$ ) or dark gray squares ( $i = 2$ ) in Fig. 2(a). Using linear spin-wave theory [26], we obtain the dispersion relation depicted as red and blue lines in Fig. 2(b), which features spin-split magnon modes. Their splitting is given by

$$\Delta E = 2\hbar^2 S (J_{\text{FM}_2} - J_{\text{FM}_1}) \left[ \cos(\sqrt{2}k_y a) - \cos(\sqrt{2}k_x a) \right]. \quad (2)$$

It is maximal and opposite along the high-symmetry lines  $\overline{\Gamma X}$  and  $\overline{\Gamma Y}$  and vanishes along the nodal lines  $\overline{\Gamma M}$ . Thus, the model exhibits the characteristic features in the magnon band structure expected in altermagnets [22, 27, 28].

The phonon Hamiltonian of the system respects the symmetry of the square lattice and comprises nearest-neighbor interaction with restoring forces along longitudinal  $K_L^{(1)}$  and transverse  $K_T$  directions with respect to the bonds as well as longitudinal next-nearest neighbor interactions  $K_L^{(2)}$ . It reads

$$\hat{H}_{\text{ph}} = \sum_i \frac{\mathbf{p}_i^2}{2M} + \sum_{\langle\langle i, j \rangle\rangle} \left[ (K_L^{(1)} - K_T) (\mathbf{u}_{ij} \cdot \hat{\mathbf{R}}_{ij})^2 + K_T \mathbf{u}_{ij}^2 \right] + \sum_{\langle\langle i, j \rangle\rangle} K_L^{(2)} (\mathbf{u}_{ij} \cdot \hat{\mathbf{R}}_{ij})^2, \quad (3)$$

where  $\mathbf{u}_{ij} = \mathbf{u}_j - \mathbf{u}_i$  and  $\mathbf{p}_i$  and  $\mathbf{u}_i$  are the momentum and position operator of an atom at lattice site  $i$ , respectively, describing the dynamics in the  $xy$  plane.  $\hat{\mathbf{R}}_{ij}$  refers to the unit bond vector between atoms at lattice sites  $i$  and  $j$ , while  $M$  is the mass of the nuclei. The phonon dispersion relation is depicted in gray in Fig. 2(b) along with the magnon modes. Note that in the structural unit cell the phonon system comprises only a single atom per unit cell forming two acoustic bands. However, since the magnetic unit cell is larger, the corresponding Brillouin

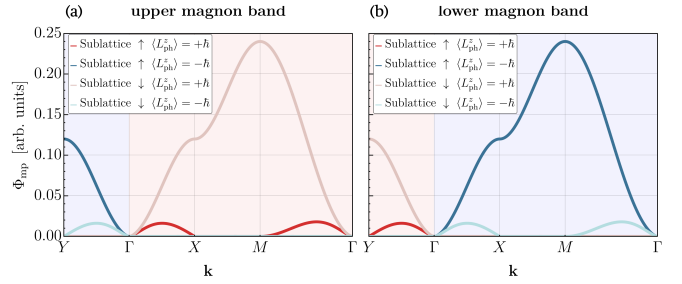


FIG. 3. Coupling strength between the (a) upper, (b) lower magnon branch and the circularly and sublattice-polarized phonon modes. The background color and the line color indicate the signs of the magnon spin and the phonon angular momentum, respectively. The matching of colors indicates the chiral selectivity of the magnon-phonon coupling  $\hat{H}_{\text{mpc}}$  [Eq. (5)]. Note that the magnon modes are degenerate along  $\overline{\Gamma M}$ .

zone is smaller and the bands have to be down-folded yielding four phonon branches. Because of the restriction to in-plane displacements, the phonon angular momentum is aligned with the  $z$  axis and can be expressed as [9]

$$L_{\text{ph}}^z = \sum_{i,p} (u_{ip}^x p_{ip}^y - u_{ip}^y p_{ip}^x). \quad (4)$$

Symmetry demands that the expectation values of  $L_{\text{ph}}^z$  vanish in an inversion- and time-reversal-symmetric (non-magnetic) square lattice [14].

For the magnon-phonon coupling we consider interfacial DMI [29, 30], which results from the breaking of the out-of-plane mirror symmetry. Denoting the DM vector as  $\mathbf{D}_{ij} = D\hat{\mathbf{R}}_{ij} \times \hat{\mathbf{z}}$ , where  $D$  is the interaction strength, the Hamiltonian  $\hat{H}_{\text{DMI}} \propto \mathbf{D}_{ij} \cdot (\mathbf{S}_i \times \mathbf{S}_j)$  does not modify the noninteracting magnon dispersion relation, as  $\mathbf{D}_{ij}$  is perpendicular to the ground state magnetization [31]. (Although the true ground state in the presence of DMI would be a noncollinear state [32], an easy-axis anisotropy would stabilize the collinear ground state for sufficiently small  $D$ . We do not implement the anisotropy for simplicity, since it does not change the qualitative effects that we discuss in the following.) The influence of the lattice excitations on the magnons enters the model by the modification of the bond vectors  $\mathbf{R}_{ij} \mapsto \mathbf{R}_{ij} + \mathbf{u}_{ij}$ . Expansion of the DMI up to first order in the displacements of the atoms yields the coupling Hamiltonian [16, 18, 26, 31]

$$\hat{H}_{\text{mpc}} = \frac{DS}{R} \sum_{\langle\langle i, j \rangle\rangle} \left\{ \pm (\mathbf{u}_i - \mathbf{u}_j) \cdot (\mathbf{S}_i - \mathbf{S}_j) \right\}. \quad (5)$$

The sum in the expression of  $\hat{H}_{\text{mpc}}$  runs over *all* next-nearest neighbors  $\langle\langle i, j \rangle\rangle$ . The “+” sign holds for those sites  $i, j$  of the  $\uparrow$  and the “-” sign for the  $\downarrow$  sublattice. We note in passing that we have neglected contributions that originate from the distance dependence of  $D(R)$  [31], which we explicitly analyze in the Supplemental Material [26].

To characterize  $\hat{H}_{\text{mpc}}$ , Fig. 3 presents the coupling strength between the magnon modes and the circularly polarized

phonons, which correspond to the eigenmodes of  $L_{\text{ph}}^z$  [Eq. (4)]. The background and the line colors indicate the sign of the magnon spin and phonon angular momentum, respectively.

For the upper magnon band [Fig. 3(a)], the magnon spin is negative along  $\bar{\Gamma}\bar{Y}$ , and the band couples exclusively to left-handed circularly polarized phonons with negative angular momentum ( $\langle L_{\text{ph}}^z \rangle = -\hbar$ ) on both sublattices. The coupling strength on the  $\downarrow$  sublattice is weaker than on the  $\uparrow$  sublattice and vanishes at the Y point. Along  $\bar{\Gamma}\bar{X}$  the magnon spin reverses sign, such that the band couples solely to right-handed circularly polarized phonons with positive angular momentum ( $\langle L_{\text{ph}}^z \rangle = \hbar$ ). Along  $\bar{\Gamma}\bar{M}$ , the two magnon branches become degenerate, rendering their labeling arbitrary. Overall,  $\hat{H}_{\text{mpc}}$  couples each magnon spin channel selectively to a single phonon circular polarization, determined by the sign of the magnon spin.

The physical origin of this selectivity can be intuitively understood from Eq. (5). In antiferromagnets and altermagnets the two magnon branches have opposite chiralities, corresponding to clockwise or counter-clockwise spin precession in the  $xy$  plane [27, 33]. The dynamic spin precession induces an effective field acting on the lattice displacements through  $\hat{H}_{\text{mpc}}$ . For co-rotating chiral phonons—those sharing the same sense of rotation—the time average of Eq. (5) remains finite. In contrast, the coupling to counter-rotating phonons averages to zero. Within a given magnon band, the sublattice amplitudes of the spin precession are generally unequal. For instance, the spin-down magnon mode exhibits a larger precession amplitude on the  $\uparrow$  sublattice, as the magnon spin is defined as the difference of the spin expectation values between the excited and the ground states [34]. As  $\mathbf{k}$  approaches the boundary of the first Brillouin zone, the amplitude of the  $\downarrow$  sublattice diminishes, while that of the  $\uparrow$  sublattice remains finite.

The dispersion relation of the coupled system

$$\hat{H} = \hat{H}_{\text{m}} + \hat{H}_{\text{ph}} + \hat{H}_{\text{mpc}} \quad (6)$$

is plotted in Fig. 4(a). Please refer to the Supplemental Material for a description of the methods [26]. Here, the color indicates the magnon/phonon/mixed character of the quasiparticles. Evidently, avoided crossings emerge at the intersection of magnon and phonon bands, giving rise to hybrid magnetic and structural excitations dubbed “magnon polarons” [35]. Furthermore, the zoom shown in Fig. 4(b) into the highlighted section as part of the  $\bar{\Gamma}\bar{Y}$  line provides insights into the generation of phonon angular momentum by magnon-phonon coupling through time-reversal symmetry breaking. In agreement with previous studies, a distinct avoided crossing pattern emerges at the intersection of two phonon bands and a single magnon band [18, 36]. While the energy and phonon character of the central mode remain unchanged, two magnon-polaron modes emerge whose energies are shifted. Additionally, the hybridization generates phonon angular momentum for the states close to the avoided crossing [cf. Fig. 4(c)]. Interestingly, we find that the phonon angular momentum changes sign and vanishes directly at the avoided crossing. Only in its vicinity it

becomes nonzero. Further analysis reveals that the sublattice-resolved phonon angular momentum is maximized directly at the avoided crossing reaching values of up to  $\hbar/2$  and that the lattice vibrations are almost fully circularly polarized [cf. Fig. 4(e), (f)]. Because the circular polarization is reversed on the two sublattices, the sublattice-resolved angular momenta partially compensate each other and the net angular momentum is strongly suppressed.

To analyze the cause of the compensation of the phonon angular momentum, we focus on the crossing of the lower magnon band with two phonon bands in Fig. 4(b). Fig. 3 indicates that the lower magnon mode couples almost exclusively to phonons on the down-sublattice ( $\downarrow$ ) and with a phonon angular momentum of  $+\hbar$ . Fig. 4(e) displays the phonon angular momentum of the  $\downarrow$  sublattice. Indeed, the magnon polaron bands exhibit a positive phonon angular momentum, while the uncoupled phonon mode has a negative phonon angular momentum. On the other hand, the opposite phonon angular momentum on the  $\uparrow$  sublattice can be explained by the phase differences between the sublattices of the crossing phonon bands.

Due to the magnetism-induced downfolding, the longitudinal acoustic crosses with the transversal optical phonon branch, for which the atoms in the unit cell oscillate in phase and out of phase, respectively. Mathematically, the phases are given by  $\exp\{i(\mathbf{k} + \mathbf{G}) \cdot \Delta\mathbf{b}\}$  where  $\Delta\mathbf{b} = \frac{a}{\sqrt{2}}(1 \ 1 \ 0)^T$  is the bond vector between the basis atoms and  $\mathbf{G}$  is either zero for the acoustic branch, or, for an optical branch, an appropriate reciprocal lattice vector of the magnetic Bravais lattice. By choosing an arbitrary  $\mathbf{k}$ -point along  $\bar{\Gamma}\bar{Y}$ , represented by  $\mathbf{k} = (0 \ k_y \ 0)^T$  and by setting  $\mathbf{G} = \left(0 \ \frac{2\pi}{\sqrt{2}a} \ 0\right)^T$ , one finds  $\mathbf{u}_{\downarrow} = \pm e^{-i\Phi} \mathbf{u}_{\uparrow}$  for the acoustic and optical branches, where  $\mathbf{u}_p$  is the wavefunction of basis atoms  $p = \uparrow, \downarrow$  and  $\Phi = -\frac{a}{\sqrt{2}}k_y$ . The longitudinal  $|l\rangle = \left(0 \ 1 \ 0 \ e^{i\Phi}\right)^T$  and transverse modes  $|t\rangle = \left(1 \ 0 \ -e^{i\Phi} \ 0\right)^T$  are linearly polarized along  $y$  and  $x$  direction, respectively. Here, we represent the wave functions in the  $(u_{\downarrow}^x, u_{\downarrow}^y, u_{\uparrow}^x, u_{\uparrow}^y)$  basis. If we now construct right-handed circularly polarized phonons ( $\langle L_{\text{ph}}^z \rangle = +\hbar$ ) on the  $\downarrow$  sublattice, the  $\uparrow$  sublattice will be left-handed circularly polarized:

$$|t\rangle + i|l\rangle = \left(1 \ i \ -e^{i\Phi} \ ie^{i\Phi}\right)^T, \quad (7)$$

and vice versa. Hence, by selectively coupling a certain circularly polarized phonon mode of the  $\downarrow$  sublattice to the magnon band, the opposite chirality is naturally imposed on the  $\uparrow$  sublattice. Since the magnon, depending on  $\mathbf{k}$ , couples to both sublattices, the phonons are not circular, but elliptical. The closer the crossing is located at the edge of the Brillouin zone, the more the magnons specifically couple to one sublattice (in this case  $\downarrow$ ) and the ellipticity is modified.

Finally, Fig. 5 depicts the total phonon angular momentum of all bands across the entire Brillouin zone. Finite phonon angular momentum emerges in the vicinity of avoided crossings between magnon and phonon bands. Since the magnon spin determines the sign of the phonon angular momentum,

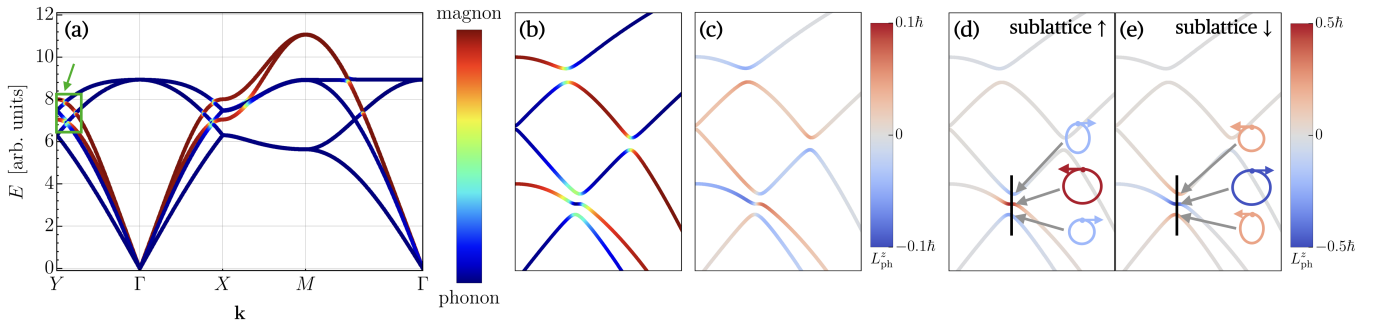


FIG. 4. Coupled magnon-phonon hybrid system. (a) Band structure of the magnon polarons along a high-symmetry path in the magnetic Brillouin zone. The color indicates the magnon/phonon character of the quasiparticles. The region highlighted by the green box and arrow is displayed in greater detail in (b)-(e). (b) Zoom of the avoided crossing pattern and quasiparticle character indicated by color. (c) Illustration of the same region but depicting the phonon angular momentum. (d), (e) Sublattice-resolved phonon angular momentum for sublattice  $\uparrow$  and sublattice  $\downarrow$ , respectively. The insets demonstrate the real-space vibrational motion (amplitude and phase) of the respective sublattices. The parameters used for the calculations are  $J_{\text{AFM}} = -1$ ,  $J_{\text{FM}_1} = 0.383$ ,  $J_{\text{FM}_2} = 0.5$ ,  $S = 1$ ,  $M = 10$ ,  $K_L^{(1)} = 160$ ,  $K_T = K_L^{(2)} = 40$ ,  $D = 0.25$ , and  $a = 1$ .

its  $k$ -space structure exhibits the  $d$ -wave character of the altermagnet – displaying an alternation of the angular momentum and vanishing ( $\langle L_{\text{ph}}^z \rangle$ ) along the nodal lines at  $\bar{\Gamma M}$ .

**Discussion and Conclusion** Our results identify altermagnets as a promising platform for realizing chiral phonons. We have reported on a mechanism of inducing a  $d$ -wave phonon angular momentum texture by coupling to magnons using the chirality-selective spin-lattice coupling. Although we have focused on a  $d$ -wave altermagnet, we expect our results to hold for  $g$ - and  $i$ -wave magnets as well, where higher-wave phonon angular momentum textures are generated. The magnetic field dependence of the magnon band structure allows for easy tunability of the phonon angular momentum texture, which makes this mechanism more flexible than the structural breaking of inversion symmetry [1, 14]. The even-parity phonon angular momentum texture lays the foundation for realizing phononic counterparts to electronic responses in altermagnets.

$d$ -wave altermagnets are known to exhibit a spin-splitter effect [37]. Based on the symmetry we can predict a *phonon angular momentum splitter effect*, where a longitudinal temperature gradient generates a transverse flow of phonon angular momentum. This effect is distinct from the phonon angular momentum Hall effect proposed by Park and Yang, since their intrinsic effect is generated by the generalized Berry curvature and does not rely on broken time-reversal symmetry [10]. In contrast, the extrinsic phonon angular momentum splitter effect arises from the anisotropic longitudinal conductivities and requires broken time-reversal symmetry [37].

In ionic crystals, the phonon angular momentum is associated with an orbital magnetic moment [38, 39]. Due to the unique symmetry of altermagnets, phonon piezomagnetism can be expected, i.e., a net phonon magnetization can be generated by strain or, conversely, the lattice can be distorted by applying a magnetic field [40, 41].

In our analysis we have focused on a particular term of the interfacial DMI, which is chirality-selective in the entire first

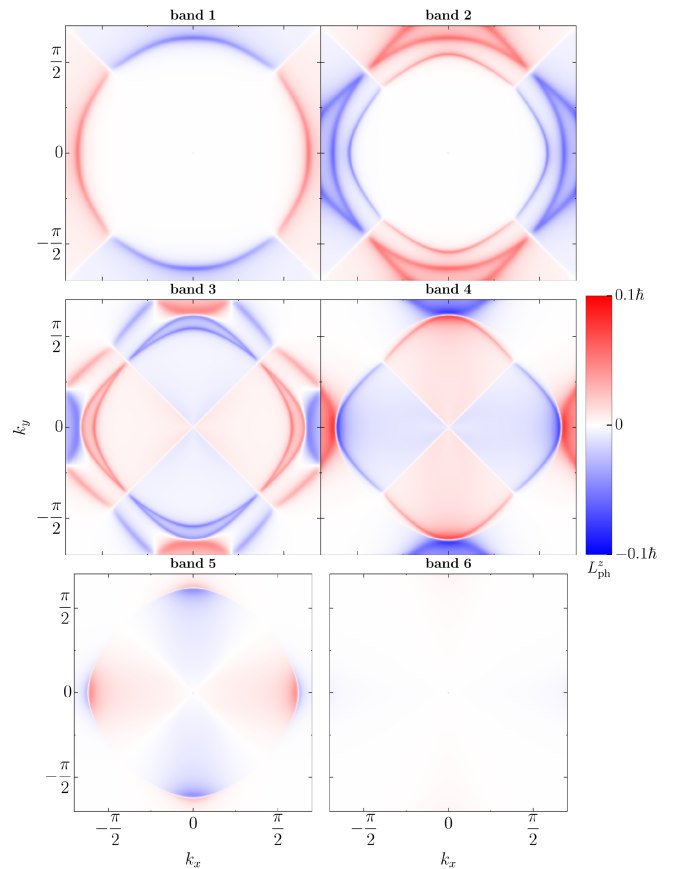


FIG. 5. Phonon angular momentum for all bands across the entire Brillouin zone. Non-zero angular momentum occurs around regions of avoided crossings and clearly reflects the  $d$ -wave character of the altermagnet. Bands are labeled in descending order starting with the highest energy. Parameters same as in Fig. 4.

Brillouin zone as we have shown using a projection of the magnetoelastic coupling onto the magnon spin and phonon angular momentum channels. The considered interfacial DMI may generate additional terms stemming from the distance dependence of  $D(R)$  lifting the perfect chiral selectivity in a  $k$  dependent fashion. While it renders the phonon angular momentum texture more complex, its general features remain robust as we demonstrate in the Supplemental Material [26]. Our projection approach can be also used to investigate other types of magnetoelastic interactions for their chiral selectivity, which can help to identify systems that maximize the phonon angular momentum and the hybridization gaps.

*Acknowledgments.* This work was funded by the German Research Foundation (DFG) as part of the German Excellence Strategy EXC3112/1 533767171 (Center for Chiral Electronics) and through TRR 277-328545488 (Project No. B04), TRR 173-268565370 (Project No. B13), and Project No. 504261060 (Emmy Noether Programme).

*Data availability.* Upon reasonable request, the data associated with this article can be made available on Zenodo [42].

---

\* Correspondence email address: [rneumann@uni-mainz.de](mailto:rneumann@uni-mainz.de)

- [1] L. Zhang and Q. Niu, Chiral Phonons at High-Symmetry Points in Monolayer Hexagonal Lattices, *Physical Review Letters* **115**, 115502 (2015).
- [2] H. Zhu, J. Yi, M.-Y. Li, J. Xiao, L. Zhang, C.-W. Yang, R. A. Kaindl, L.-J. Li, Y. Wang, and X. Zhang, Observation of chiral phonons, *Science* **359**, 579 (2018).
- [3] T. Wang, H. Sun, X. Li, and L. Zhang, Chiral Phonons: Prediction, Verification, and Application, *Nano Letters* **24**, 4311 (2024).
- [4] D. A. Garanin and E. M. Chudnovsky, Angular momentum in spin-phonon processes, *Physical Review B* **92**, 024421 (2015).
- [5] J. J. Nakane and H. Kohno, Angular momentum of phonons and its application to single-spin relaxation, *Physical Review B* **97**, 174403 (2018).
- [6] S. R. Tauchert, M. Volkov, D. Ehberger, D. Kazenwadel, M. Evers, H. Lange, A. Donges, A. Book, W. Kreuzpaintner, U. Nowak, and P. Baum, Polarized phonons carry angular momentum in ultrafast demagnetization, *Nature* **602**, 73 (2022).
- [7] M. S. Mrudul, M. Weißenhofer, and P. M. Oppeneer, *Generation of Phonons with Angular Momentum During Ultrafast Demagnetization* (2025), arXiv:2504.16547 [cond-mat].
- [8] C. Dornes, Y. Acremann, M. Savoini, M. Kubli, M. J. Neugebauer, E. Abreu, L. Huber, G. Lantz, C. A. F. Vaz, H. Lemke, E. M. Bothschafter, M. Porer, V. Esposito, L. Rettig, M. Buzzi, A. Alberca, Y. W. Windsor, P. Beaud, U. Staub, D. Zhu, S. Song, J. M. Glowina, and S. L. Johnson, The ultrafast Einstein–de Haas effect, *Nature* **565**, 209 (2019).
- [9] L. Zhang and Q. Niu, Angular Momentum of Phonons and the Einstein–de Haas Effect, *Physical Review Letters* **112**, 085503 (2014).
- [10] S. Park and B.-J. Yang, Phonon Angular Momentum Hall Effect, *Nano Letters* **20**, 7694 (2020).
- [11] K. An, A. N. Litvinenko, R. Kohno, A. A. Fuad, V. V. Naletov, L. Vila, U. Ebels, G. De Loubens, H. Hurdequint, N. Beaulieu, J. Ben Youssef, N. Vukadinovic, G. E. W. Bauer, A. N. Slavin, V. S. Tiberkevich, and O. Klein, Coherent long-range transfer of angular momentum between magnon Kittel modes by phonons, *Physical Review B* **101**, 060407 (2020).
- [12] D. M. Juraschek, R. M. Geilhufe, H. Zhu, M. Basini, P. Baum, A. Baydin, S. Chaudhary, M. Fechner, B. Flebus, G. Grissonnanche, A. I. Kirilyuk, M. Limeshko, S. F. Maehrlein, M. Mignolet, S. Murakami, Q. Niu, U. Nowak, C. P. Romao, H. Rostami, T. Satoh, N. A. Spaldin, H. Ueda, and L. Zhang, Chiral phonons, *Nature Physics*, 1 (2025).
- [13] H. Chen, W. Wu, S. A. Yang, X. Li, and L. Zhang, Chiral phonons in kagome lattices, *Physical Review B* **100**, 094303 (2019).
- [14] S. Coh, Classification of materials with phonon angular momentum and microscopic origin of angular momentum, *Physical Review B* **108**, 134307 (2023).
- [15] K. Ishito, H. Mao, Y. Kousaka, Y. Togawa, S. Iwasaki, T. Zhang, S. Murakami, J.-i. Kishine, and T. Satoh, Truly chiral phonons in  $\alpha$ -HgS, *Nature Physics* **19**, 35 (2023).
- [16] B. Ma and G. A. Fiete, Antiferromagnetic insulators with tunable magnon-polaron Chern numbers induced by in-plane optical phonons, *Physical Review B* **105**, L100402 (2022).
- [17] J. Cui, E. V. Boström, M. Ozerov, F. Wu, Q. Jiang, J.-H. Chu, C. Li, F. Liu, X. Xu, A. Rubio, and Q. Zhang, Chirality selective magnon-phonon hybridization and magnon-induced chiral phonons in a layered zigzag antiferromagnet, *Nature Communications* **14**, 3396 (2023).
- [18] Q. Wang, S. Liu, M.-Q. Long, and Y.-P. Wang, Regulation of magnon-phonon coupling by phonon angular momentum in two-dimensional systems, *Physical Review B* **108**, 174426 (2023).
- [19] J. D. Mella, L. E. F. F. Torres, and R. E. Troncoso, Chiral magnon-polaron edge states in Heisenberg-Kitaev magnets, *Physical Review B* **110**, 104433 (2024).
- [20] H. Ning, T. Luo, B. Ilyas, E. V. Boström, J. Park, J. Kim, J.-G. Park, D. M. Juraschek, A. Rubio, and N. Gedik, *Spontaneous emergence of phonon angular momentum through hybridization with magnons* (2024), arXiv:2410.10693 [cond-mat].
- [21] Q. Wang, M.-Q. Long, and Y.-P. Wang, Magnetic moments of chiral phonons induced by coupling with magnons, *Physical Review B* **110**, 024423 (2024).
- [22] M. Weißenhofer and A. Marmodoro, Atomistic spin dynamics simulations of magnonic spin Seebeck and spin Nernst effects in altermagnets, *Physical Review B* **110**, 094427 (2024).
- [23] L. Šmejkal, J. Sinova, and T. Jungwirth, Beyond Conventional Ferromagnetism and Antiferromagnetism: A Phase with Nonrelativistic Spin and Crystal Rotation Symmetry, *Physical Review X* **12**, 031042 (2022).
- [24] L. Šmejkal, J. Sinova, and T. Jungwirth, Emerging Research Landscape of Altermagnetism, *Physical Review X* **12**, 040501 (2022).
- [25] T. Jungwirth, R. M. Fernandes, E. Fradkin, A. H. MacDonald, J. Sinova, and L. Šmejkal, Altermagnetism: An unconventional spin-ordered phase of matter, *Newton* **1**, 100162 (2025).
- [26] See Supplemental Material [INSERT URL] for a description of the mathematical framework, the derivation of the magnon-phonon coupling from interfacial DMI, and additional results for alternative magnon-phonon couplings. The Supplemental Material cites Refs. [43–48].
- [27] L. Šmejkal, A. Marmodoro, K.-H. Ahn, R. González-Hernández, I. Turek, S. Mankovsky, H. Ebert, S. W. D’Souza, O. Šipr, J. Sinova, and T. Jungwirth, Chiral Magnons in Altermagnetic RuO<sub>2</sub>, *Physical Review Letters* **131**, 256703 (2023).
- [28] D. Jost, R. B. Regmi, S. Sahel-Schackis, M. Scheufele, M. Neuhaus, R. Nickel, F. Yakhou, K. Kummer, N. Brookes, L. Shen, G. L. Dakovski, N. J. Ghimire, S. Geprägs, and M. F. Kling, *Chiral Altermagnon in MnTe* (2025), arXiv:2501.17380

- [cond-mat].
- [29] I. Dzyaloshinsky, A thermodynamic theory of “weak” ferromagnetism of antiferromagnetics, *Journal of Physics and Chemistry of Solids* **4**, 241 (1958).
- [30] T. Moriya, Anisotropic Superexchange Interaction and Weak Ferromagnetism, *Physical Review* **120**, 91 (1960).
- [31] X. Zhang, Y. Zhang, S. Okamoto, and D. Xiao, Thermal Hall Effect Induced by Magnon-Phonon Interactions, *Physical Review Letters* **123**, 167202 (2019).
- [32] F. J. dos Santos, M. dos Santos Dias, and S. Lounis, Modeling spin waves in noncollinear antiferromagnets: Spin-flop states, spin spirals, skyrmions, and antiskyrmions, *Physical Review B* **102**, 104436 (2020).
- [33] S. M. Rezende, A. Azevedo, and R. L. Rodríguez-Suárez, Introduction to antiferromagnetic magnons, *Journal of Applied Physics* **126**, 151101 (2019).
- [34] N. Okuma, Magnon Spin-Momentum Locking: Various Spin Vortices and Dirac magnons in Noncollinear Antiferromagnets, *Physical Review Letters* **119**, 107205 (2017).
- [35] Y. Li, C. Zhao, W. Zhang, A. Hoffmann, and V. Novosad, Advances in coherent coupling between magnons and acoustic phonons, *APL Materials* **9**, 060902 (2021).
- [36] M. Weißenhofer, P. Rieger, M. S. Mrudul, L. Mikadze, U. Nowak, and P. M. Oppeneer, Truly Chiral Phonons Arising From Chirality-Selective Magnon-Phonon Coupling (2024), [arXiv:2411.03879](https://arxiv.org/abs/2411.03879) [cond-mat].
- [37] R. González-Hernández, L. Šmejkal, K. Výborný, Y. Yahagi, J. Sinova, T. Jungwirth, and J. Železný, Efficient Electrical Spin Splitter Based on Nonrelativistic Collinear Antiferromagnetism, *Physical Review Letters* **126**, 127701 (2021).
- [38] D. M. Juraschek and N. A. Spaldin, Orbital magnetic moments of phonons, *Physical Review Materials* **3**, 064405 (2019).
- [39] N. Shabala, F. Tietjen, and R. M. Geilhufe, *Axial phonomagnetic effects* (2025).
- [40] C. R. W. Steward, R. M. Fernandes, and J. Schmalian, Dynamic paramagnon-polarons in altermagnets, *Physical Review B* **108**, 144418 (2023).
- [41] P. A. McClarty and J. G. Rau, Landau Theory of Altermagnetism, *Physical Review Letters* **132**, 176702 (2024).
- [42] H. Bendin, A. Mook, I. Mertig, and R. R. Neumann, D-Wave Angular Momentum Texture in Altermagnets by Magnon-Phonon Hybridization, Zenodo (2025), <https://doi.org/10.5281/zenodo.17550609>.
- [43] T. Holstein and H. Primakoff, Field Dependence of the Intrinsic Domain Magnetization of a Ferromagnet, *Physical Review* **58**, 1098 (1940).
- [44] J. H. P. Colpa, Diagonalization of the quadratic boson hamiltonian, *Physica A: Statistical Mechanics and its Applications* **93**, 327 (1978).
- [45] R. Shindou, R. Matsumoto, S. Murakami, and J.-i. Ohe, Topological chiral magnonic edge mode in a magnonic crystal, *Physical Review B* **87**, 174427 (2013).
- [46] R. R. Neumann, *Theoretical Prediction for Probing Magnon Topology*, Ph.D. thesis, Martin-Luther-Universität Halle-Wittenberg, Halle (Saale) (2024).
- [47] U. Bissbort, W. Hofstetter, and D. Poletti, Operator-based derivation of phonon modes and characterization of correlations for trapped ions at zero and finite temperature, *Physical Review B* **94**, 214305 (2016).
- [48] C. P. Romao, R. Catena, N. A. Spaldin, and M. Matas, Chiral phonons as dark matter detectors, *Physical Review Research* **5**, 043262 (2023).